



Contents lists available at SciVerse ScienceDirect

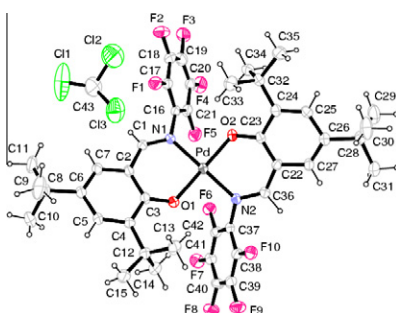
## Spectrochimica Acta Part A: Molecular and Biomolecular Spectroscopy

journal homepage: [www.elsevier.com/locate/saa](http://www.elsevier.com/locate/saa)Polyfluorinated Pd(II)-3,5-di-*tert*-butylsalicylaldimenes complexes: Synthesis, structure, spectroscopy, redox behaviors and catalytic activityVeli T. Kasumov<sup>a,\*</sup>, Ertan Sahin<sup>b</sup><sup>a</sup> Department of Chemistry, Harran University, Fac. Arts & Sci., 63300 Şanlıurfa, Turkey<sup>b</sup> Department of Chemistry, Ataturk University, Fac. Sci., TR-25240 Erzurum, Turkey

## HIGHLIGHTS

- ▶ New bis(*N*-polyfluorophenyl-3,5-Bu<sub>2</sub>-salicylaldiminato)palladium(II) complexes.
- ▶ Spectroscopic, redox reactivity and catalytic activity of the above complexes are reported.
- ▶ Bis-[*N*-(3,5-di-*tert*-butylsalicylidene)-2,3,4,5,6-pentafluoroaniline]Pd(II) has been structurally characterized.

## GRAPHICAL ABSTRACT



## ARTICLE INFO

## Article history:

Received 22 July 2012

Received in revised form 29 December 2012

Accepted 10 January 2013

Available online 23 January 2013

## Keywords:

Bis[*N*-(3,5-di-*tert*-butylsalicylidene)-

polyfluorophenyl]Pd

X-ray structure

Redox reactivity

Pd<sup>II</sup>-phenoxy radicals

## ABSTRACT

A series of new polyfluorinated palladium(II) complexes (**7–12**) of *N*-polyfluorophenyl-3,5-di-*tert*-butylsalicylaldimines (**1–6**) have been synthesized. They were characterized by analytical, spectroscopic (UV/Vis, IR, <sup>1</sup>H NMR, and ESR), electrochemical methods and their chemical oxidation and hydrogenation catalytic activity were studied. The X-ray crystal structure analysis of bis[*N*-(3,5-di-*tert*-butylsalicylidene)-F<sub>5</sub>Ph]Pd(II) (**12**) revealed a slightly distorted square-planar *trans*-PdN<sub>2</sub>O<sub>2</sub> geometry around the palladium center. The UV/Vis and EPR results indicate that chemical oxidation of **7–10** by Ce(IV) in CHCl<sub>3</sub> generates relatively stable Pd(II)-phenoxy radical complexes ( $g = 2.0044–2.0062$ ). The results of chemical and electrochemical oxidation of **1–12**, as well as the catalytic activity of **7–10** complexes in the hydrogenation of PhNO<sub>2</sub> were presented.

© 2013 Elsevier B.V. All rights reserved.

## Introduction

The design, synthesis and structural characterization of salicylaldimine complexes bearing sterically hindered *tert*-butyl groups are a subject of current interest due to their interesting structural, magnetic, spectral, catalytic and redox properties, use as models for enzymes and various theoretical interests [1–4]. The discovery of Cu(II)-phenoxy radical centers in the active site of Cu<sup>II</sup>-containing enzymes (galactose and glyoxal oxidases and others) has stimulated the development of various transition metal chelates that

have ability to form the directly coordinated M<sup>II,III</sup>-phenoxy radical complexes [3–7].

One of the unique properties of first row-transition metal complexes with phenoxyimine ligands bearing bulky *tert*-butylated phenol fragments is their ability to form stable metal(II/III)-phenoxy type radical complexes [2–4]. 4- and 5-group transition metal complexes with above mentioned ligands have been widely used as olefin polymerization catalysts [8–15]. Among these catalysts, the use of perfluorinated phenoxyimine ligands with transition metal complexes (fluorinated M–F catalysts) to catalyze the ethylene and propylene living polymerization reactions has become one of the most widely used compounds in highly controlled living olefin polymerization catalysts [8–15]. Fujita and co-workers

\* Corresponding author. Tel.: +90 414 318 3588; fax: +90 414 3440051.

E-mail address: [vkasumov@harran.edu.tr](mailto:vkasumov@harran.edu.tr) (V.T. Kasumov).

demonstrated that bulky substituents *ortho* to the phenoxy-oxygen in these complexes play a key role in achieving both living and isospecific polymerization and increase their catalytic activity [12–14]. Calculations demonstrate that the *ortho*-F interacts electronically with a  $\beta$ -H on a growing polymer chain (*ortho*-F/ $\beta$ -H distance: 2.276 Å) [14–16]. This indicates that the presence of an attractive interaction between the *ortho*-F and the  $\beta$ -H for all *ortho*-fluorinated Ti–FI independent of the phenoxy-imine ligand structures, confirming the generality of the unusual attractive interaction for *ortho*-F in Ti–FI catalysts.

In continuation, in our studies on the chemistry of bulky phenoxyimine ligands bearing di-*tert*-butylated phenol fragments we report the synthesis, crystal structure, spectroscopic characterization, chemical oxidation and catalytic activity of the *N*-perfluorophenyl-3,5-di-*tert*-butylsalicylalimine ligands Pd(II) complexes [17–20]. The aim of this work is to investigate the influence of the strong electron-withdrawing fluorine atoms in the aniline ring on the formation of Pd(II)-phenoxy radicals and catalytic activity in the hydrogenation of nitro compounds. Here we describe the synthesis, crystal structure, spectroscopic characterization as well as chemical and electrochemical redox behaviors and catalytic activity of some *N*-polyfluorophenyl-3,5-di-*tert*-butylsalicylidene ligands (**1–6**) Pd(II) complexes (**7–12**) (Scheme 1). The crystal structure of **2** and **3** ligands [21] and some spectral and redox behavior of complex **10** [22], as well as the synthesis and some IR and  $^1\text{H}$  NMR characteristics of **1–6** ligands [8–13] have been early reported.

## Experimental

### Materials

Chemicals, reagents, and solvents employed were commercially available and used as received. All chemicals, reagents, and solvents employed were commercially available and used as received. *N,N*-dimethylformamide (DMF), dimethyl-ulfoxide (DMSO), acetonitrile (MeCN), chloroform, ethanol, methanol, 2,4-di-*tert*-butylphenol, hexamethylenetetramine, nitrobenzene, palladium(II) acetate,  $(\text{NH}_4)_2\text{Ce}(\text{NO}_3)_6$  (CAN), acetic acid and all fluorinated anilines (2,4-difluoroaniline, 2,5-difluoroaniline, 2,6-difluoroaniline, 2,3,4-trifluoroaniline, 2,3,5,6-tetrafluoroaniline and 2,3,4,5,6-pentafluoroaniline) were purchased from Sigma–Aldrich and used without further purification. 3,5-*t*Bu<sub>2</sub>-salicylaldehyde was prepared according to a published procedure [23].

### Instrumentation

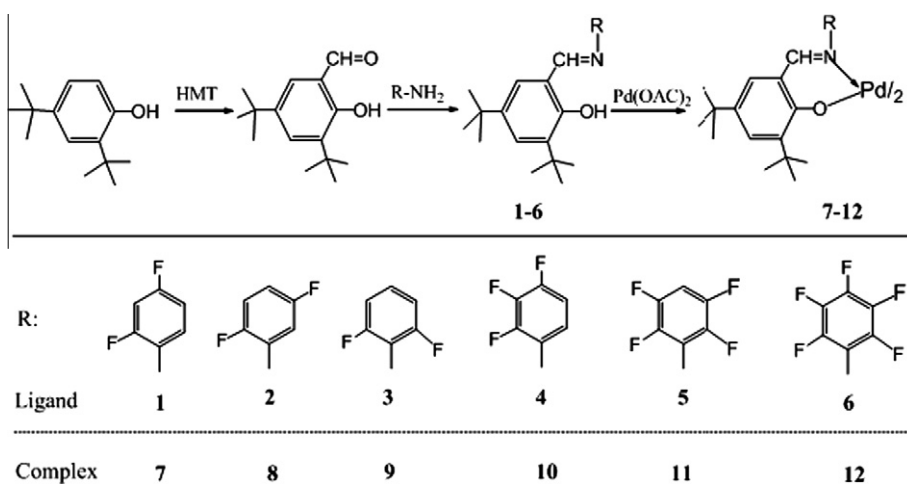
The C, H, N elemental analyses were performed on a LECO CHNS-932 model analyzer. Electronic spectra were recorded by using a Perkin Elmer Lambda 25 spectrometer, IR spectra obtained on a Perkin Elmer FT-IR spectrometer using KBr pellet.  $^1\text{H}$  NMR spectra were measured on a Bruker Spectro spin Avance DPX-300 Ultra Shield Model NMR with Me<sub>4</sub>Si as an internal standard in CDCl<sub>3</sub> solutions ESR spectra were taken on a Varian E109C X-band spectrometer. The field and frequency calibration were made using DPPH ( $g = 2.0037$ ). An Eco Chemie Autolab-12 potentiostat with the electrochemical software package GPES 4.9 (Utrecht, The Netherlands) was used for voltammetric measurements. A platinum disk (2 mm o.d.) was employed as a working electrode, a platinum coil as a counter electrode, and an Ag/AgCl as reference electrode, respectively. All measurements were performed in MeCN containing 0.05 M Et<sub>4</sub>NBF<sub>4</sub> (TEA-TFB) as a supporting electrolyte under N<sub>2</sub> at ambient temperatures.

### Synthesis

General method for the synthesis of *N*-(3,5-di-*tert*-butylsalicylidene)polyfluoroaniline ligands. The compounds **1–4** were prepared by the standard method of condensation of 3,5-di-*tert*-butyl-2-hydroxybenzaldehyde with corresponding fluoroanilines in absolute ethanol in the presence of a few drops of formic acid. The mixture was stirred at reflux for 24–30 h and then the volume of the solution was reduced to ca. 25 ml. After cooling to room temperature, a yellow solid precipitate was isolated by vacuum filtration and dried in air to give **1–4** (62–88%) products. The ligands **5** and **6** were prepared by similar manners using excess of 2,3,5,6-tetrafluoroaniline and 2,3,4,5,6-pentafluoroaniline according the literature procedure [24]. The  $^1\text{H}$  NMR and elemental analysis data of the **1–6** ligands were found to be identical with those reported by Fujita and co-workers [8–15].

### Synthesis of palladium(II) complexes

The general method of preparation was as follows. Palladium acetate (0.25 mmol) was added to a stirred warm solution ( $\sim 40^\circ\text{C}$ ) containing 0.5 mmol of appropriate ligand (**1–4**) in 30 ml of acetonitrile. The mixture was heated for about 50 min at this temperature and left at room temperature for 3–4 h. The



Scheme 1. A general synthetic route for the palladium(II) complexes; HMT = hexamethylenetetramine.

precipitated red complex was collected by suction filtration and washed with water, could methanol and recrystallised from methanol/chloroform mixture. The synthesis of complexes **11** and **12** was carried out in the same way as that described for above complexes, but 10 ml glacial acetic acid was used instead of acetonitrile. The crude orange red solid complexes **11** and **12** were recrystallized in methanol/CHCl<sub>3</sub> mixture.

#### Hydrogenation procedure

The hydrogenation of nitrobenzene was carried out in a thermostatic reaction flask (100 ml) at 25 °C under 760 Torr H<sub>2</sub> with vigorous stirring in dry and deoxygenated 25 ml DMF solution. Catalyst (1.0 × 10<sup>-5</sup> to 4.0 × 10<sup>-6</sup> mol) was added into 25 ml DMF and saturated with H<sub>2</sub> for 10–15 min. After addition of NaBH<sub>4</sub> (5 × 10<sup>-6</sup> mol) the mixture was stirred for ca. 5 min and PhNO<sub>2</sub> (4–8 × 10<sup>-4</sup> mol) was transferred into the vessel. Then the H<sub>2</sub> gas was bubbled again into the flask and the volume of the absorbed H<sub>2</sub> was measured periodically.

#### X-ray crystallography

For the crystal structure determination, the single-crystals of the complexes (**12**·CHCl<sub>3</sub>) were used for data collection on a four-circle Rigaku R-Axis RAPID-S diffractometer (equipped with a two-dimensional area IP detector). The graphite-monochromatized Mo K $\alpha$  radiation ( $\lambda = 0.71073 \text{ \AA}$ ) and oscillation scans technique with  $\Delta\omega = 5^\circ$  for one image were used for data collection. The lattice parameters were determined by the least-squares methods on the basis of all reflections with  $F^2 > 2\sigma(F^2)$ . Integration of the intensities, correction for Lorentz and polarization effects and cell refinement was performed using Crystal Clear (Rigaku/MSI Inc., 2005) software [25]. The structures were solved by direct methods using SHELXS-97 [26] and refined by a full-matrix least-squares procedure using the program SHELXL-97 [26]. H atoms were positioned geometrically and refined using a riding model. The final difference Fourier maps showed no peaks of chemical significance.

## Results and discussion

#### IR and UV/visible spectroscopic characterization of 7–12 compounds

The analytical, IR, <sup>1</sup>H NMR spectroscopic characteristics of the compounds **1–6** were previously reported [8–10,13]. The analytical, IR, <sup>1</sup>H NMR spectroscopic characteristics of the compounds **7–12** is presented in Supplemental part. In order to compare the spectral properties of the ligands and their **7–12** complexes, also we have measured the IR and <sup>1</sup>H NMR characteristics of **1–6** ligands. The IR spectra of all compounds exhibit sharp bands in the region of 2860–2950 cm<sup>-1</sup> due to the asymmetric and symmetric  $\nu(\text{C}-\text{H})$  stretching frequencies of the C(CH<sub>3</sub>)<sub>3</sub> groups. The  $\nu(\text{C}=\text{N})$  stretching vibrations of **7–12** are blue shifted (1602–1616 cm<sup>-1</sup>) relative to those of free **1–6** ligands (1622–1630 cm<sup>-1</sup>), indicating coordination of the imine nitrogen atom to copper(II) (Section 'Experimental'). A weak broad feature centered at 2500–2800 cm<sup>-1</sup>, due to  $\nu(\text{OH})$  of the intramolecularly H-bonded OH...N in **1–6**, disappears in the spectra of all the complexes. This suggests their coordination *via* deprotonated phenolic oxygen atom to Pd(II). The appearance of new bands at 1526–1530 cm<sup>-1</sup>, attributable to the coordinated  $\nu(\text{C}-\text{O})$  stretching mode [27,28] and in the 450–660 cm<sup>-1</sup> region assignable to the Pd–O and Pd–N bonds, further confirmed the coordination of ligands through phenolic O and azomethine N atoms.

The electronic spectra of **1–6** (Table 1, Figs. 1 and 2a), unlike many other non-fluorinated bidentate arylsalicylaldimines [20,27,28], did not exhibit absorptions above 370 nm even in the concentrated strongly H-bonding polar solvents such as ethanol and methanol solutions. This observation suggests that the perfluorinated **1–6** salicylaldimines exist only in enol-imine tautomer form at room temperature. The higher intense absorption bands observed in the ranges of 210–330 and 355–362 nm (Table 1) have been assigned to  $\pi \rightarrow \pi^*$  and  $n \rightarrow \pi^*$  transitions for the electrons localized on the aromatic and imine groups, respectively. However, a more intense band at 355–362 nm, according to their higher extinction coefficients ( $\epsilon = 10,000\text{--}39,000 \text{ M}^{-1}\text{cm}^{-1}$ ) can be assigned to overlapped bands originated from low intense  $n \rightarrow \pi^*$  transitions and higher intense charge transfer absorptions [28]. Thus, UV/Vis study in the different solvents indicates that no tautomerism takes place in polar

**Table 1**  
Electronic spectral data for **1–12** and their oxidized intermediates.

Compound	Solvent	Electronic spectra, $\lambda$ (nm), ( $\log \epsilon$ , $\text{M}^{-1}\text{cm}^{-1}$ )
<b>1</b>	MeOH	207(4.83), 222*, 235*, 277(4.35), 325*, 356(4.21)
	MeCN	222(4.6), 235**, 277(4.4), 309(4.12), 322 (4.1)*, 355(3.98)
<b>2</b>	MeCN + Ox.	222, 275, 308, 320*, 354, 520*
	MeOH	208(4.7), 220(4.6), 281(4.5), 314(4.5), 329*, 360(4.3)
	EtOH	210(4.8), 224(4.8), 237*, 281(4.7), 331*, 362(4.3)
	MeCN	221(4.5), 235*, 280(4.4), 314(4.4), 329*, 358(4.2)
<b>3</b>	MeCN + Ox.	268, 285*, 315, 328*, 350
	MeOH	208(4.9), 227(4.8), 276(4.8), 305(4.4), 321(4.6), 356(4.5)
	EtOH	218*, 233(4.9), 276(4.8), 306(4.7), 320(4.6), 357 (4.5)
<b>4</b>	MeCN	227(3.3), 276(3.2), 305(3.1), 320(3.1), 355(2.9)
	MeCN + Ox	272, 308, 320*, 352, 420*, 520*
	MeOH	207(4.8), 222(4.7), 236**, 282(4.6), 306(4.6), 323*, 358(4.6)
	MeCN	223(4.6), 333**, 282(4.47), 306(4.5), 322*, 357(4.3)
<b>5</b>	MeCN + Ox.	278, 305, 320*, 355, 550**
	MeOH	206(4.6), 231(4.5), 278(4.4), 305(4.3), 361(4.1)
	MeCN	229(4.5), 280(4.4), 306*(4.33), 321**, 360(4.1)
<b>6</b>	MeCN + Ox	230*, 277, 305*, 322*, 355, 715
	MeOH	206(4.8), 225(4.8), 279(4.7), 300(4.6), 322*, 361(4.4)
<b>7</b>	MeCN	224(4.46), 279(4.34), 323*(4.19), 360(4.05)
	MeCN + Ox	277, 304*, 322*, 736
	EtOH	208(4.6), 239*(4.5), 263(4.6), 303(4.3), 414(3.7)
	CHCl <sub>3</sub>	263(4.8), 306(4.5), 414(3.9)
<b>8</b>	MeCN	241(4.93), 262(4.98), 302(4.65), 409(4.19)
	MeCN + Ox	235*, 289, 350, 404*, 530**
	EtOH	210(4.5), 237(4.6), 264(4.6), 303(4.3), 353*(4.2), 420(4.2)
	CHCl <sub>3</sub>	261(4.97), 306(4.62), 421(4.08)
<b>9</b>	MeCN	238(4.5), 262(4.6), 303(4.28), 416(3.7)
	MeCN + Ox	250*, 294, 320*, 378, 405
	EtOH	219(4.7), 252(4.0), 301(4.9), 354(3.3), 422(3.4)
	CHCl <sub>3</sub>	259(4.17), 305(3.91), 358*(3.10), 422(3.56)
	MeCN	220(4.5), 262(4.54), 302(4.3), 416(3.72)
<b>10</b>	MeCN + Ox	237, 261*, 296, 355*, 413, 530**
	EtOH	237*(4.52), 263(4.55), 302(4.26), 417(3.78)
	CHCl <sub>3</sub>	262(4.83), 306(4.76), 420(4.09)
	MeCN	240*(4.1), 262(4.13), 302(3.98), 414(3.47)
<b>11</b>	MeCN + Ox	234*, 294, 348*, 404* 500**
	EtOH	240(4.77), 260(4.89), 304(4.48), 430(3.98)
	CHCl <sub>3</sub>	258(3.62), 307(4.67), 432(4.03)
	MeCN	240(4.57), 261(4.86), 305(4.57), 426(4.06)
<b>12</b>	MeCN + Ox	238*, 296, 355*, 419
	EtOH	208(4.7), 241(4.9), 262(4.9), 306(4.7), 430(4.2)
	CHCl <sub>3</sub>	269(4.9), 308(4.8), 430(4.2)
	MeCN	240(4.8), 261(4.9) 305(4.5), 426(4.0)
	MeCN + Ox	231, 299, 355, 419

\* Shoulder.

\*\* Very weak shoulder.

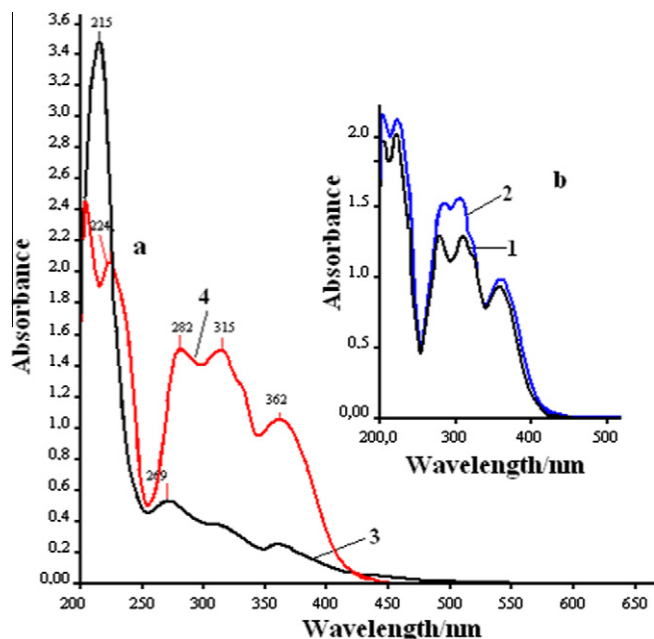


Fig. 1. Electronic spectra of 1–4 ligands in EtOH: (a) spectra of 3 and 4. (b) Inset: spectra of 1 and 2.

H-bonding solvents for *N*-perfluorinated 3,5-di-*tert*-butyl-salicylaldimines.

#### <sup>1</sup>H NMR spectral characterization of 7–12 compounds

The <sup>1</sup>H NMR spectral data was obtained for 7–10 complexes in CDCl<sub>3</sub>, with their assignments are presented in Section 'Experimental'. In order to establish the mode of coordination of the ligands on the metal center, <sup>1</sup>H NMR proved to be very useful. The comparison of the <sup>1</sup>H NMR chemical shifts of 1–6 hydrogen atoms with those in the corresponding 7–12, shows that all proton signals of the ligands were shifted to upfield in the spectra of corresponding complexes. For example,  $\delta$  8.71–8.88 (CH=N),  $\delta$  1.50–1.52 [3-C(CH<sub>3</sub>)<sub>3</sub>] and  $\delta$  1.35–1.37 ppm [5-C(CH<sub>3</sub>)<sub>3</sub>] of the free 1–6 ligands groups protons signals are, respectively, shifted upfield to  $\delta$  7.53–8.08 (CH=N),  $\delta$  1.23–1.25 [3-C(CH<sub>3</sub>)<sub>3</sub>] and 0.87–0.90 ppm [5-C(CH<sub>3</sub>)<sub>3</sub>] regions, in the spectra of corresponding 7–12 complexes (Section 'Experimental'). The OH proton signals in the <sup>1</sup>H NMR

spectra of the free ligands ( $\delta$  11.45–14.86 ppm) disappeared in the complexes indicating that the OH group was deprotonated and bonded to the metal ion as an oxygen anion (Section 'Experimental'). Note that the chemical shift of OH proton decreased with an increase in the number of F atoms on the aniline ring in the order  $\delta$  = 13.42 (1) > 13.35 (3) > 13.32 (2) > 13.18 (4) > 12.84 (5) > 12.76 (6). The higher field shift trends were also detected for salicylic and aniline rings protons. Similar magnetic shielding effects have been previously observed in Schiff base complexes of Pd(II), Zn(II), Co(II) and Cu(II) [20,28]. A plausible explanation upfield shift of the peripherally bonded CH<sub>3</sub> protons is that when the *tert*-butyl group is exposed to the anisotropy generated by close proximity to an aromatic ring, the group is shielded and an upfield shift is observed [28].

Complexes 7–12 are diamagnetic, suggesting a square-planar geometry for these complexes. Electronic spectra of these complexes are also indicative of a square-planar geometry [18,20,27]. The electronic spectra of 7–12 in EtOH, MeCN and CHCl<sub>3</sub> solutions exhibit very similar three intense bands in the 260–432 nm region (Table 1). The intense broad band appeared within 409–432 nm due to its higher molar extinction coefficients ( $\epsilon$  = 2512–15,850 M<sup>-1</sup> cm<sup>-1</sup>) is assigned to metal-to-ligand charge-transfer [21,23].

#### Chemical oxidation of 1–12

Our previous studies demonstrated that the chemical oxidation of some bis[*N*-alkyl(aryl)-3,5-*t*-Bu<sub>2</sub>-salicylaldiminato] M(II) (M = Cu, Co, Pd) complexes by (NH<sub>4</sub>)<sub>2</sub>[Ce(NO<sub>3</sub>)<sub>6</sub>] (CAN) in CHCl<sub>3</sub> or MeCN was accompanied by disappearance of their *d-d* bands and appearance of the new absorptions typical for radical signals [2–4,19].

The addition of 1.5 equiv. CAN to CHCl<sub>3</sub> solution of 7–10 complexes under ambient conditions caused a color change from orange red to dark red and EPR monitoring of these reaction mixture revealed the appearance of signals at  $g$  = 2.0032–2.0062 typical for phenoxy radical species (Fig. 3). For oxidized 7, 8, 9 and 10 complexes isotropic single line spectra with  $g$  = 2.0062 ( $\Delta H_{pp}$  = 6.25 G),  $g$  = 2.0059 ( $\Delta H_{pp}$  = 6.0 G),  $g$  = 2.0044 ( $\Delta H_{pp}$  = 6.0 G) and  $g$  = 2.0054 ( $\Delta H_{pp}$  = 6.5 G), respectively, were detected (Fig. 3a). These spectral features are similar to other M(II)-phenoxy radicals [3,19]. It is interesting that when 4-fold excess of CAN was added to CHCl<sub>3</sub> solution of 10 instead of single line spectrum the six line spectrum (Fig. 3b) with  $g$  = 2.0032 and line width  $\Delta H_{pp}$  = 23.5 G was detected. It is necessary to note that the above detected radicals are unstable and upon second scanning the decrease about 50% in their peak intensities was observed.

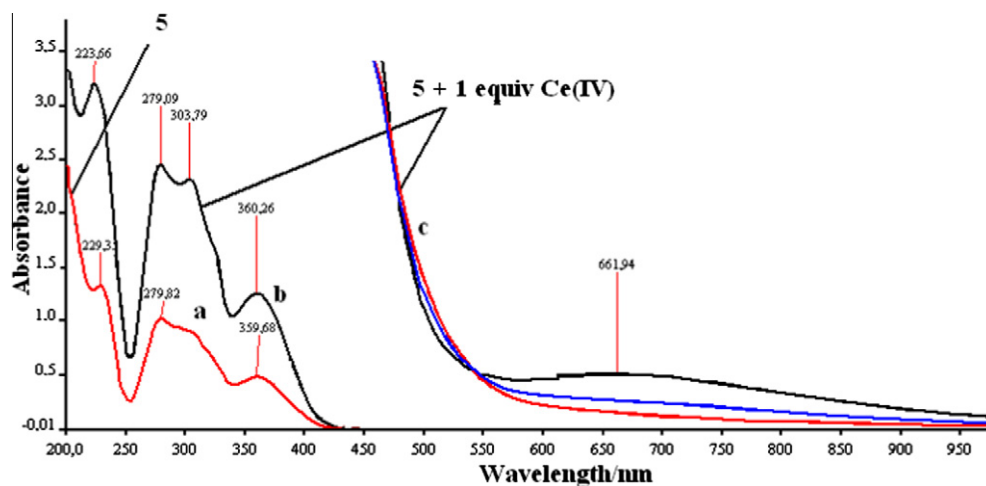
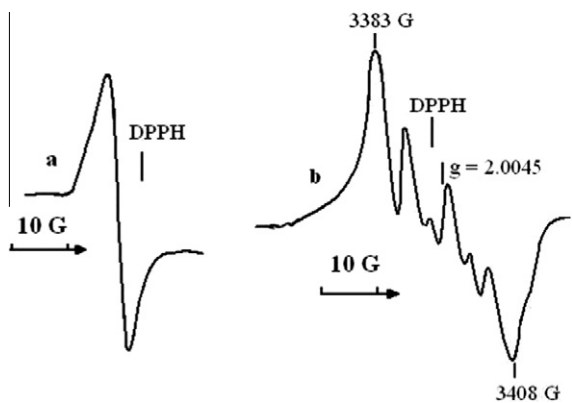


Fig. 2. Spectral changes in the oxidation of 5 with one equiv. Ce(IV). Spectra of ligand 5 (a) and its oxidized species (b and c) in acetonitrile and at r.r.



**Fig. 3.** Solution ESR spectra generated by the chemical oxidation of **7** (a) and **10** (b) complexes with Ce(IV) in  $\text{CHCl}_3$  at r.t. and aerobic conditions: (a) **7** + 1.5 equiv. Ce(IV) and (b) **10** + 4 equiv. Ce(IV).

The UV/Vis spectral results of the oxidized compounds along with non-oxidized **1–12** original compounds in MeCN are collected in Table 1. The spectral changes followed by the chemical oxidation of **1–12** with one-electron oxidant, CAN, in  $\text{CH}_3\text{CN}$  solutions at r.t. and under aerobic conditions, were monitored by UV/Vis

spectroscopy in the range 200–1100 nm. The results of these experiments show that on mixing of equivalent molar amounts of the ligands **1–6** and CAN in MeCN, the light yellow color of the ligands simultaneously turns to greenish-brown and except **2**, the appearance of a new broad absorption in the range 520–736 nm was detected in the spectra of the reaction mixture (Table 1). The shoulder patterns at 520–550 nm for oxidized [**1–4**]<sup>+</sup> and a broad maximum bands at 715 and 736 nm in the spectra of the oxidized [**5**]<sup>+</sup> and [**6**]<sup>+</sup>, respectively, confirm the generation of the phenoxyl radical species, which are relatively stable at r.t. under aerobic conditions. Similar spectral changes were also observed upon one-electron oxidation for all **7–12** complexes in MeCN. The comparison of the UV/Vis spectra of **7–12** with those for oxidized [**7–12**]<sup>+</sup> species revealed the appearance new bands within 355–380 and 500–550 nm regions for oxidized complexes (Fig. 4, Table 4). These new absorption features along with EPR results clearly indicate that chemical oxidation of **7–12** complexes generate Pd(II)-phenoxyl radical species.

#### Electrochemical oxidation of **7–12** complexes

The electrochemical redox behaviors of **7–12** has been examined by cyclic voltammetry technique using a Pt working electrode

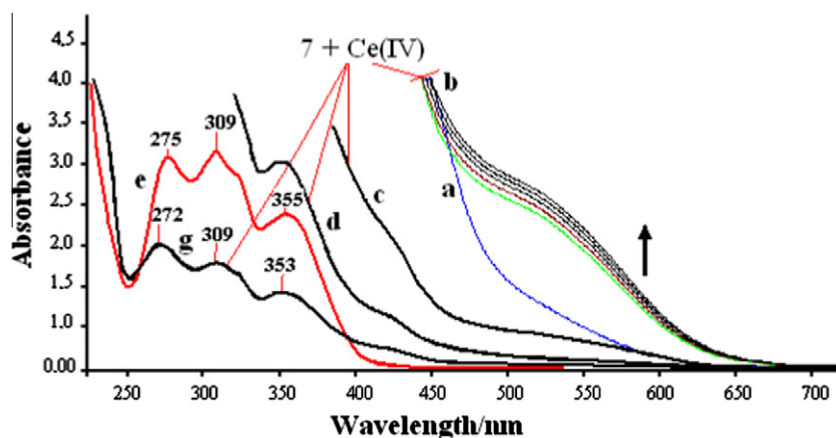


**Fig. 4.** The changes in the UV/Vis spectra of **7** (a and e) and **7** + Ce(IV) system (b–d, g) in MeCN solution at r.t. and aerobic conditions; (a) – initial spectrum of **7**; (b) – successive scanned spectra of **7** + Ce(IV) mixture; (c, d, g) – diluted spectrum of (a). The arrow indicates the direction of the increasing absorbance.

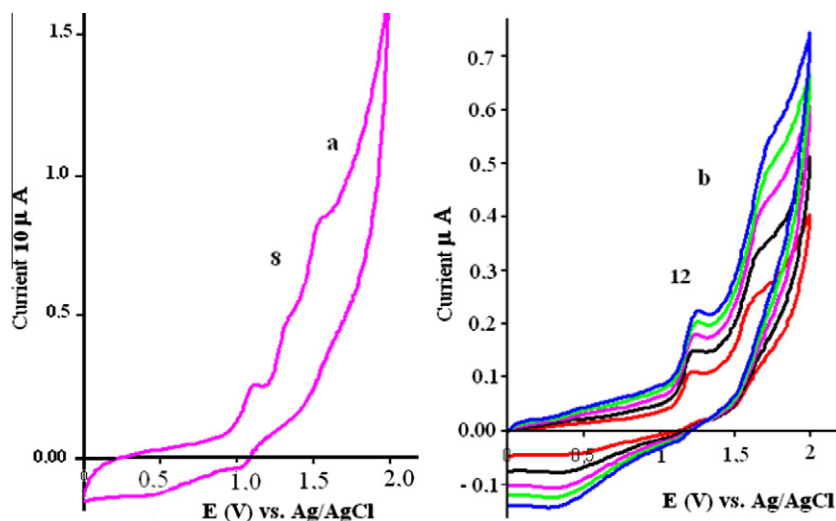


**Fig. 5.** Cyclic voltammograms of **8** and **12** in MeCN containing 0.05 M TEATFB in the potential range 0.0–2.0 V: (a) CV of **8** (0.4 mM) at a scan rate of 0.05 V/s. (b) CV of **12** (0.5 mM) at a scan rate of 0.1–0.5 V/s. Working electrode Pt, Counter electrode Pt wire, reference electrode Ag/AgCl was used in all experiments.

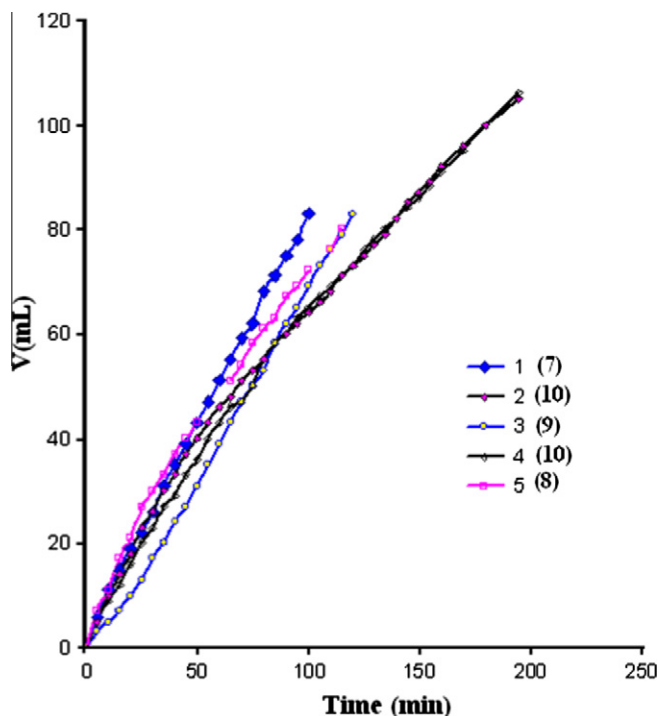


**Fig. 6.** Hydrogenation of PhNO<sub>2</sub> with catalysts **7–9** ( $3 \times 10^{-4}$  M,  $6 \times 10^{-6}$  mol) at 298 K, in the presence of a catalytic amount of NaBH<sub>4</sub> ( $2.5 \times 10^{-6}$  mol) in DMF. **2 (10)** and **4 (10)** were measured in the absence of NaBH<sub>4</sub>. **4 (10)** was measured after 72 h of the **2 (10)**.

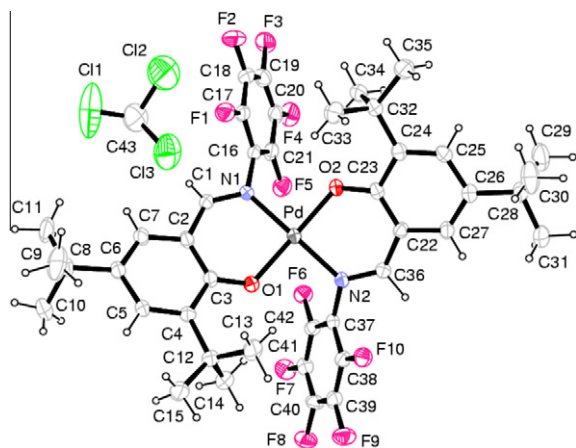


**Fig. 7.** Perspective view of the Pd(II) complex (**12-CHCl<sub>3</sub>**) with the atom numbering scheme. Displacement ellipsoids are at the 40% probability level.

in acetonitrile (MeCN) in the potentials ranging from  $-2.0$  to  $+2.5$  V versus Ag/AgCl at 293 K under N<sub>2</sub> containing Et<sub>4</sub>NBF<sub>4</sub> (0.05 M) as the background electrolyte. The CV of **7** exhibits three irreversible ligand centered anodic oxidation processes with anodic peak potentials ( $E_{pa}$ ) approximately at 1.08, 1.35, 1.50 V versus Ag/AgCl indicating the instability of the oxidized species in the CV time scale. The first oxidation wave of the **8** and **9** complexes are quasi-reversible with  $E_{pa}^1/E_{pc}^1$  of 1.14/1.01 and 1.15/1.08 V, respectively. The second and third waves are irreversible oxidation processes the respective anodic peak potentials at ca 1.32 and 1.58 V for former and at 1.48 and 1.58 V versus Ag/AgCl for latter complexes, respectively (Fig. 5a). On the other hand, for complex **10** under above conditions only one quasi-reversible oxidation wave with  $E_{pa}^1/E_{pc}^1 = 1.14/0.32$  was detected. It is interesting that

**Table 2**

Crystallographic data of the complex **12-CHCl<sub>3</sub>**.

Empirical formula	C <sub>42</sub> H <sub>42</sub> N <sub>2</sub> O <sub>2</sub> F <sub>10</sub> Pd ···CHCl <sub>3</sub>
Formula weight	1022.6
Temperature (K)	293(2)
Crystal size (mm)	0.21 × 0.14 × 0.11
Crystal system	Monoclinic
Space group	P2 <sub>1</sub> /n
<i>a</i> (Å)	13.6334(3)
<i>b</i> (Å)	13.1863(4)
<i>c</i> (Å)	25.5649(8)
$\alpha = \gamma$ (°)	90
$\beta$ (°)	92.114 (3)
<i>V</i> (Å <sup>3</sup> )	4592.56(2)
<i>Z</i>	4
$\rho$ calcd. (g/cm <sup>3</sup> )	1.48
$\mu$ (mm <sup>-1</sup> )	0.656
<i>F</i> (000)	2071.8
$\theta$ – range (°)	2.2–26.4
Index ranges	–17 < <i>h</i> < 17, –16 < <i>k</i> < 13, –31 < <i>l</i> < 31
Reflections collected	26364
Reflections observed (>2 $\sigma$ )	9231
Data/restraints/parameters	4627/0/565
<i>R</i> <sub>1</sub> (all)	0.089
w <i>R</i> <sub>2</sub>	0.218
Goof	1.033

**Table 3**

Selected bond lengths (Å) and angles (°) for (**12-CHCl<sub>3</sub>**).

Selected bond lengths (Å)			
Pd–O(1)	2.004(6)	Pd–O(2)	1.979(6)
Pd–N(1)	2.011(7)	Pd–N(2)	2.008(6)
F(6)–C(42)	1.340(10)	F(1)–C(17)	1.312(12)
F(7)–C(41)	1.339(11)	F(4)–C(20)	1.330(13)
O(1)–C(3)	1.314(9)	O(2)–C(23)	1.317(10)
F(3)–C(19)	1.350(12)	N(1)–C(16)	1.425(10)
N(1)–C(1)	1.289(10)	F(2)–C(18)	1.351(14)
Selected Bond angles (°)			
O(1)–Pd–O(2)	170.1(3)	O(1)–Pd–N(1)	92.0(3)
O(1)–Pd–N(2)	89.1(3)	O(2)–Pd–N(1)	88.7(3)
O(2)–Pd–N(2)	91.7(3)	N(1)–Pd–N(2)	170.6(3)
Pd–O(1)–C(3)	124.6(5)	Pd–O(2)–C(23)	123.3(5)
Pd–N(1)–C(16)	122.4(5)	Pd–N(1)–C(1)	121.8(6)
C(16)–N(1)–C(1)	115.2(7)	Pd–N(2)–C(37)	119.9(5)

**Table 4**

Parameters (Å) for hydrogen bonds and short intramolecular contacts.

<i>D</i> –H... <i>A</i>	<i>H</i> ... <i>A</i>	<i>D</i> ... <i>A</i>	< <i>D</i> –H... <i>A</i>
C(14)–H(14B)···Cg(4)	2.67	3.431(11)	136
C(34)–H(34C)···Cg(2) <sup>i</sup>	2.68	3.435(11)	135
C(43)–H(43)···Cg(1) <sup>ii</sup>	2.49	3.449(19)	166
<i>Y</i> – <i>X</i> ...Cg( $\pi$ -ring)			
C(43)–Cl(3)···Cg(2) <sup>iii</sup>	3.538(8)	4.559(7)	118
C(21)–F(5)···Cg(4) <sup>iv</sup>	3.434(7)	4.256(8)	119
C(41)–F(7)···Cg(3) <sup>iv</sup>	3.181(6)	4.380(8)	148

Symmetry codes: (i) *x, y, z*; (ii)  $3/2 - x, -1/2 + y, 1/2 - z$ ; (iii)  $-1/2 + x, 1/2 - y, 1/2 + z$ ; (iv)  $1 - x, 1 - y, -z$  Cg(1), Cg(2), Cg(3) and Cg(4), are the centroid of the rings C(2)–C(7), C(16)–C(21), C(22)–C(27), and C(37)–.

the CV profile of **11** and **12** complexes (Fig. 5b) are very similar to each other and significantly different from those for **7–10** complexes. The positive slope obtained in the plot of the peak current ( $i_p$ ) versus the square root of the voltage scan rate ( $V^{1/2}$ ) within the range of 100–500 mV/s indicates diffusion controlled electron exchange reactions at the first oxidation peak potentials of the **11** and **12** complexes [29].

Analyses of the electrochemical results show that the potentials of the ligand-centered redox couple do not correlate with the electron withdrawing ability of the F atoms on the aniline ring substituents. Some voltammograms also exhibit ill-defined low intense

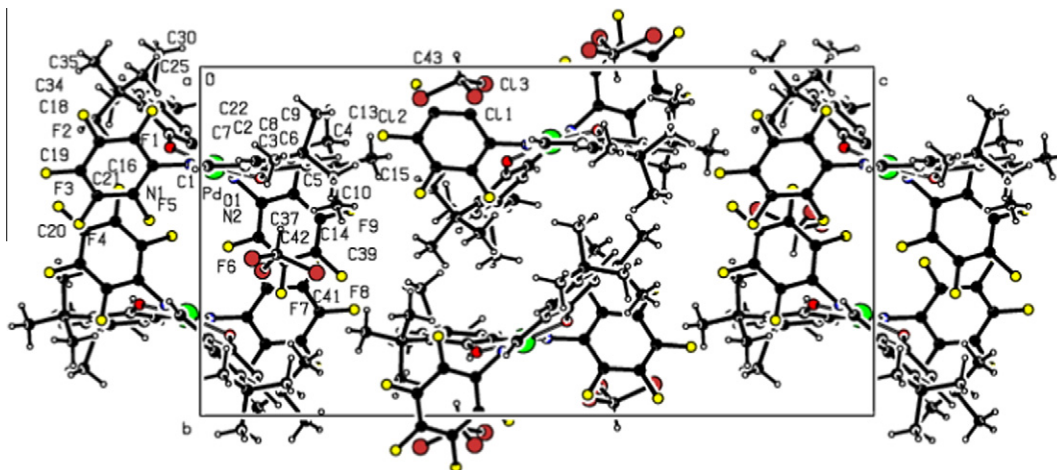


Fig. 8. Unit cell packing diagram for **12**-CHCl<sub>3</sub> along the *a*-axis.

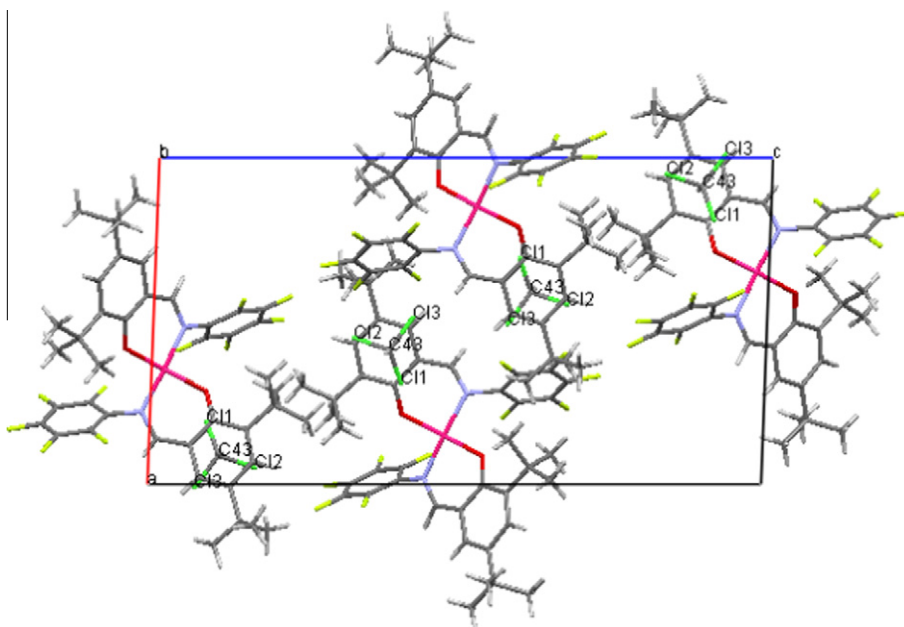


Fig. 9. C–H...Cg(π-ring) stacking interaction with the chloroform and the C(16)–C(21) aromatic ring along the unit cell diagonal-axis.

minor features, which can be assigned to the Pt-surface adsorbed phenoxy radicals or to other secondary decomposition products.

#### Catalytic reduction of nitrobenzene by complexes **7–10**

The present investigation has shown that all of the **7–10** complexes exhibit catalytic activity in the hydrogenation of nitrobenzene under normal pressure of H<sub>2</sub>, 760 Torr, in DMF solution at 25 °C. Nitrobenzene, as identified by means of IR scanning, was completely reduced to aniline. The catalytic studies showed that complexes **7–10** exhibit a catalytic activity towards the hydrogenation of nitrobenzene in DMF solution at 25 and 30 °C, under normal pressure of H<sub>2</sub> gas (760 Torr), without any preliminary activation. The concentration of nitrobenzene was varied from 0.147 to 1.224 mol/l using a fixed amount of the catalyst ( $4 \times 10^{-4}$  mol/l) Pd(II) content. The course of the hydrogenation of the PhNO<sub>2</sub> with **7–10** catalysts is shown in Fig. 6. Although, for starting of the hydrogenation of PhNO<sub>2</sub> with **7–9** catalysts it is necessary to add of NaBH<sub>4</sub> ( $1.0 \times 10^{-6}$  mol) to catalysts solution

for acceleration their catalytic activity, for complex **10** did not need any preliminary activation. In order to check whether the catalyst lost its activity or not, the recycling efficiency of the catalysts was carried out by conducting some experiments over a period of 36 h. It was observed that the initial rate of hydrogenation reaction remains almost unchanged even after two weeks for complex **10**. The recycling experiments showed that the catalytic activity of **10** remains unchanged and can be re-used without appearance any sign of decomposition of complex. Unlike nonfluor substituted Pd(*N*-X-arylsalicylaldimato)<sub>2</sub> type complexes [20], no evidence of the palladium metal precipitation was observed in the course of the hydrogenation of nitrobenzene for a period of two weeks. The average rate of H<sub>2</sub> absorption and the specific catalytic activity of **7–10** were obtained as 0.5–1.1 ml/min and 3.56–6.58 H<sub>2</sub> consumed/mol-cat (min), respectively. While the hydrogenation catalytic activity of the present Pd(II) complexes are lower than those for some mono-F, Br and CH<sub>3</sub> substituted Pd(*N*-X-arylsalicylaldimato)<sub>2</sub> type complexes [20], the catalytic activity of **9** and **10** complexes remains unchanged at least two weeks.

### Crystal structure of **12**·CHCl<sub>3</sub>

In spite of our best efforts, suitable crystals for X-ray diffraction of **7–11** complexes could not be obtained. But our efforts are continued. The molecular structure of solvated Pd(II) complex **12**·CHCl<sub>3</sub> including atom-numbering is shown in Fig. 7. Crystal data and additional data collection parameters and refinement details are presented in Table 2. Selected bond distances and angles as well as the data of hydrogen-bonding interactions are given in Tables 3 and 4, respectively. Complex **12**·CHCl<sub>3</sub> adopts a slightly distorted square-planar *trans*-[PdN<sub>2</sub>O<sub>2</sub>] coordination geometry with O–Pd–O, N–Pd–N and O–Pd–N angles ranges of 88.73(8)–170.56(8)°. The search in the CSD database [30] revealed that for complexes formed with the similar ligands, most of them have the *trans*-N<sub>2</sub>O<sub>2</sub> square-planar geometry around Pd(II) center. The Pd(II) bonds to the two phenolic oxygen and the two imine nitrogen atoms of **12**·CHCl<sub>3</sub> with a Pd–O distances of 1.979(2), 2.004(2) Å and Pd–N distances of 2.008(3), 2.0011(3) Å, respectively are close to those known for Pd(II) salicylaldimine complexes [31–34]. The C36–N2 [1.310(4) Å] and C1–N1 [1.289(4) Å] distances indicate that these correspond to double bonds. The dihedral angle between the two coordination planes defined by Pd–N1–O1 and Pd–N2–O2 is 36.45(15)° (Fig. 7), as well as the *trans*-O2–Pd–O1 and *trans*-N2–Pd–N1 bond angles are 170.09(4) Å and 170.56(5) Å, respectively, indicate that the Pd(II) center has a distorted square-planar geometry. The *cis*-N1–Pd–O1 and O2–Pd–N2 bond angles are 92.03(5)° and 91.74(8)°, respectively. The dihedral angle between salicylidine ring plane (C2–C7, Ring A) and Pd/N1/O1 plane is 19.2(3)°, while the same angle between the other salicylidine ring plane (C22–C27, Ring B) and Pd/N2/O2 plane is 20.0(2)°. The angle between the planes of pentafluorobenzene moieties is 47.2(2)°, whereas the dihedral angle between the salicylidine planes is 47.8(3)°. The C3/O1/Pd and C23/O2/Pd angles are 124.6(2)° and 123.3(2)°, respectively, as expected for sp<sup>2</sup>-hybridized oxygen atom. Within the layer the shortest non-bridged Pd···Pd distance is 8.617 Å. In extended structure, there is non-classical hydrogen bonding interactions (Fig. 8). But weak π–π interactions are observed, shortest distance between the aromatic rings (C37–C42) and (C16–C21)<sup>i</sup> [symmetry code (i): 1 – x, 1 – y, – z] centroids is 5.328(6) Å. The C–H...Cg (π-ring) stacking interaction with the chloroform and the C(16)–C(21) aromatic ring along the unit cell diagonal-axis is presented in Fig. 9. In the packing structure of **12**·CHCl<sub>3</sub>, there are also a weak intermolecular C–H···π, C–Cl···π and C–F···π interactions (Fig. 8 and Table 4). These intermolecular interactions, namely an extensive network of non-classical hydrogen bonds, π–π stacking and π–ring interactions, are responsible for constructing an infinite 3D lattice in the crystal structure of **12**·CHCl<sub>3</sub>.

### Conclusions

A new series of polyfluorinated palladium(II) complexes with *N*-perfluorophenyl-3,5-di-*tert*-butyl-salicylaldimine ligands were synthesized and characterized by spectroscopic and X-ray crystallography, and examined their chemical and electrochemical oxidation behaviors as well as catalytic activity in hydrogenation reaction. The X-ray study shows that the geometry around palladium(II) atoms is a slightly distorted square planar. UV–Vis and <sup>1</sup>H NMR spectra revealed that the *N*-polyfluorophenyl-

3,5-di-*tert*-butylsalicylaldimines exist only in the enol-imine form. Electron-withdrawing fluorine atoms in F<sub>n</sub>Ph groups increase the magnetic shielding of all proton atoms in the **7–12** complexes. As supported by EPR and UV/Vis studies, chemical oxidation of the presented complexes with Ce(IV) leads to the formation of the relatively stable Pd(II)-phenoxy radicals at ambient conditions. It has been demonstrated that **7–10** complexes exhibit moderate catalytic activity in the hydrogenation of nitrobenzene without losing activity at least for two weeks.

### Acknowledgements

Support of this investigation by Harran University Research Council for Grants under HUBAK-712 and HUBAK-1043 and Ataturk University, Erzurum, is gratefully acknowledged.

### Appendix A. Supplementary material

Supplementary data associated with this article can be found, in the online version, at <http://dx.doi.org/10.1016/j.saa.2013.01.015>.

### References

- [1] C.G. Pierpont, C.W. Lnge, Prog. Inorg. Chem. 41 (1994) 331–442.
- [2] P. Chaudhuri, K. Wieghardt, Prog. Inorg. Chem. 50 (2001) 151–216.
- [3] B.A. Jazdzewski, W.B. Tolman, Coord. Chem. Rev. 200 (2000) 633–685.
- [4] J.W. Whittaker, Chem. Rev. 103 (2003) 2347–2364.
- [5] J. Stubbe, W.A. van der Donk, Chem. Rev. 98 (1998) 705–762.
- [6] V.C. Gibson, S.K. Spitzmesser, Chem. Rev. 103 (2003) 283–315.
- [7] L. Canali, D.C. Sherrington, Chem. Soc. Rev. 28 (1999) 85–93.
- [8] H. Makio, N. Kashiwa, T. Fujita, Adv. Synth. Catal. 344 (2002) 477–493.
- [9] R. Furuyama, J. Saito, S. Ishii, H. Makio, M. Mitani, H. Tanaka, T. Fujita, J. Organomet. Chem. 690 (2005) 4398–4413.
- [10] H. Makio, H. Terao, I. Washita, T. Fujita, Chem. Rev. 111 (2011) 2363–2449.
- [11] A.F. Mason, G.W. Coates, J. Am. Chem. Soc. 126 (2004) 16326–16327.
- [12] A. Sakuma, M.S. Weiser, T. Fujita, Polym. J. 39 (2007) 193–207.
- [13] M. Mitani, R. Furuyama, J. Mohri, J. Saito, S. Ishii, H. Terao, T. Nakano, H. Tanaka, T. Fujita, J. Am. Chem. Soc. 125 (2003) 4293–4305.
- [14] T. Matsugi, T. Fujita, Chem. Soc. Rev. 37 (2008) 1264–1277.
- [15] K. Kawai, T. Fujita, Top. Organomet. Chem. 26 (2009) 3–46.
- [16] A. Sakuma, M.S. Weiser, T. Fujita, Polym. J. 39 (2007) 193–207.
- [17] A.A. Medjidov, V.T. Kasumov, M.K. Guseynova, H.S. Mamedov, V.S. Aliev, Dokl. AN USSR 259 (1981) 866–869.
- [18] V.T. Kasumov, A.A. Medjidov, Koord. Khim. 15 (1989) 1404–1407.
- [19] V.T. Kasumov, F. Köksal, A. Sezer, Polyhedron 24 (2005) 1203–1211.
- [20] V.T. Kasumov, F. Köksal, S.Ö. Yaman, Polyhedron 24 (2005) 319–325.
- [21] Ö. Celik, V.T. Kasumov, E. Sahin, Acta Crystallogr. E65 (2009) o2786.
- [22] V.T. Kasumov, I. Ucar, A. Bulut, J. Fluorine Chem. 131 (2010) 59–65.
- [23] J.F. Larrow, E.N. Jacobsen, Y. Gao, Y. Hong, X. Nie, C.M. Zepp, J. Org. Chem. 59 (1994) 1939–1942.
- [24] M. Mitani, J. Mohri, Y. Yoshida, J. Saito, S. Ishii, K. Tsuru, S. Matsui, R. Furuyama, T. Nakano, H. Tanaka, S. Kojoh, T. Matsugi, N. Kashiwa, T. Fujita, J. Am. Chem. Soc. 124 (2002) 3327–3336.
- [25] Rigaku/MS, Inc., 9009 New Trails Drive, The Woodlands, TX.
- [26] G.M. Sheldrick, SHELXS97 and SHELXL97, University of Göttingen, Germany, 1997.
- [27] V.T. Kasumov, F. Köksal, R. Köseoglu, J. Coord. Chem. 57 (2004) 591–603.
- [28] S.J. Gruber, C.M. Harris, E. Sinn, J. Inorg. Nucl. Chem. 30 (1968). 1805–183.
- [29] R.S. Nicholson, I. Shain, Anal. Chem. 36 (1964) 706–723.
- [30] F.H. Allen, Acta Crystallogr. B58 (2002) 380–388.
- [31] H. Zhang, D.W. Norman, T.M. Wentzell, A.M. Irving, J.P. Edwards, S.L. Wheaton, C.M. Vogels, S.A. Westcott, F.J. Baerlocher, A. Decken, Trans. Met. Chem. 30 (2005) 63–68.
- [32] E.G. Bowes, G.M. Lee, C.M. Vogels, A. Dickent, S.A. Westcott, Inorg. Chim. Acta 377 (2011) 84–90.
- [33] V.W. Day, M.D. Glick, J.L. Hoard, J. Am. Chem. Soc. 90 (1968) 4803–4808.
- [34] Y.S. Uh, H. Zhang, C.M. Vogels, A. Decken, S.A. Westcott, Bull. Korean Chem. Soc. 25 (2004) 986–990.